Physics of Fluids ARTICLE scitation.org/journal/phf

# Mpemba effect in molecular gases under nonlinear drag

Cite as: Phys. Fluids 32, 072010 (2020); doi: 10.1063/5.0016243
Submitted: 2 June 2020 • Accepted: 4 July 2020 •
Published Online: 22 July 2020



Andrés Santos[1,a] and Antonio Prados[2,b]

## AFFILIATIONS

[1] Departamento de Física and Instituto de Computación Científica Avanzada (ICCAEx), Universidad de Extremadura, 06006 Badajoz, Spain
[2] Física Teórica, Universidad de Sevilla, Apartado de Correos 1065, 41080 Sevilla, Spain

**Note:** This paper is part of the Special Topic, Advances in Micro/Nano Fluid Flows: In Memory of Prof. Jason Reese.
[a] **Author to whom correspondence should be addressed:** andres@unex.es
[b] **Electronic mail:** prados@us.es

## ABSTRACT

We look into the Mpemba effect—the initially hotter sample cools sooner—in a molecular gas with nonlinear viscous drag. Specifically, the gas particles interact among them via elastic collisions and with a background fluid at equilibrium. Thus, within the framework of kinetic theory, our gas is described by an Enskog–Fokker–Planck equation. The analysis is carried out using the first Sonine approximation, in which the evolution of temperature is coupled to that of excess kurtosis. This coupling leads to the emergence of the Mpemba effect, which is observed at an early stage of relaxation and when the initial temperatures of the two samples are close enough. This allows for the development of a simple theory, linearizing the temperature evolution around a reference temperature, namely, the initial temperature closer to the asymptotic equilibrium value. The linear theory provides a semiquantitative description of the effect, including expressions for crossover time and maximum temperature difference. We also discuss the limitations of our linearized theory.



## I. INTRODUCTION

One of the signatures of nonequilibrium systems is the presence of memory effects.[1] A system displays memory when its time evolution from a given initial state is not uniquely determined by the initial values of its macroscopic—or hydrodynamic—variables. In other words, the system evolution depends on how it has been previously aged; memory effects are thus intimately related to aging,[2] which has been typically associated with glassy behavior.[3–7] Notwithstanding this, in addition to being investigated in models for glasses,[8–11] it has been found in many different physical systems: granular fluids,[12,13] dense granular matter,[14,15] ferroelectrics,[16] disordered mechanical systems,[17] and frictional interfaces,[18] to name just a few.

The Mpemba effect[19–24] is a counterintuitive memory phenomenon: given two samples of fluid, the one that is initially hotter may cool more rapidly. Therefore, the curves describing the time evolution of the temperature of the two samples cross each other at a certain time $t_c$, and the curve for the initially hotter sample stays below the other one for longer times, $t > t_c$. It is important to characterize the range of values of the relevant physical quantities that allow for the emergence of the Mpemba effect; in general, the difference in initial temperatures must be small enough.

Although first reported in the case of water,[19,25] its existence for that liquid is still controversial.[26,27] As a proof of concept, the feasibility of the Mpemba effect has recently been reported in granular gases.[21,28–30] Therein, collisional inelasticity couples the evolution of (granular) temperature to other quantities—such as the kurtosis or the rotational-to-translational energy ratio—monitoring the nonequilibrium nature of the velocity distribution function (VDF), even in homogeneous and isotropic states.[31,32]

In this work, we show that the Mpemba effect is also present in homogeneous and isotropic states of molecular gases—i.e., with elastic collisions—driven by an external drag force with a velocity-dependent friction coefficient. The particles of our system are supposed to be hard spheres, for the sake of simplicity, surrounded by a background fluid in equilibrium. Gas particles collide among

them, with these collisions being modeled by a Boltzmann–Enskog collision term in the evolution equation for the VDF.

Gas particles also interact with the background fluid. This interaction translates into two forces: (i) a macroscopic, deterministic, nonlinear drag force and (ii) a stochastic force. The intensity of the latter follows from the fluctuation–dissipation theorem, which ensures that the gas VDF tends to a Maxwellian with the temperature of the background fluid in the long-time limit. In the evolution equation, the interaction between the gas and the fluid is described by a Fokker–Planck term; therefore, the VDF obeys an Enskog–Fokker–Planck equation with nonlinear drag.

The framework of our work is thus nonlinear Brownian motion,[33] but the Brownian particles are no longer independent since they interact through instantaneous hard collisions. If the particles of the background fluid, with mass $m_{\text{bf}}$, are much lighter than the Brownian particles, with mass $m$, the drag force is usually assumed to be linear in the velocity of the particles, $\boldsymbol{F}_{\text{drag}} = -m\zeta_0\boldsymbol{v}$. In fact, this is the leading behavior found when an expansion in powers of $m_{\text{bf}}/m$ is performed, which leads to linear Brownian motion. Nevertheless, the drag force becomes nonlinear when higher order terms in the expansion are brought to bear. Specifically, the drag force can be written as $\boldsymbol{F}_{\text{drag}} = -m\zeta(v)\boldsymbol{v}$, and there appears a velocity-dependent drag coefficient $\zeta(v)$, with $\zeta(v=0) = \zeta_0$. Therein, the first correction in $\zeta_0$ introduces a quadratic dependence on $v$.[34–36] In some situations, nonlinearities in the drag coefficient have quite strong physical implications.[36–40]

The main goal of this paper is to study the Mpemba effect in the kinetic theory framework we have just described, i.e., the Enskog–Fokker–Planck equation with nonlinear drag. To meet this end, we work using the first Sonine approximation, in which the time evolution of temperature is coupled to that of excess kurtosis. This coupling, which is absent in the case of $\zeta(v) = \zeta_0$, is responsible for the emergence of the Mpemba effect. The value of excess kurtosis is assumed to be small in the Sonine approximation, which entails that the initial temperatures of the samples must be close to each other and the Mpemba crossover takes place at the early stage of relaxation. This allows us to linearize the problem and derive analytical expressions for the relevant physical quantities that characterize the Mpemba effect, like the crossing time in the temperature evolution, the maximum value of the initial temperature difference, and the magnitude of the effect.

The plan of the paper is as follows. We put forward the model and the kinetic description in Sec. II, where the equations for the velocity moments are also derived. Section III is devoted to the Sonine approximation: the infinite hierarchy for the velocity moments is closed by expanding the VDF in Laguerre polynomials, retaining only the first nontrivial cumulant, namely, excess kurtosis. The Mpemba effect is analyzed in Sec. IV: we develop a linearized model, investigate the crossover time, construct the phase diagram in the space of parameters, quantify the magnitude of the effect, and finally study the accuracy of the linearized theory. Finally, Sec. V presents the main conclusions of our work.

## II. ENSKOG–FOKKER–PLANCK EQUATION: MOMENT EQUATIONS

Let us consider a $d$-dimensional system of elastic hard spheres of mass $m$ and diameter $\sigma$ in a uniform and isotropic fluidized state. The spheres are assumed to be suspended in a background fluid in equilibrium so that their one-body VDF $f(\boldsymbol{v})$ satisfies the Enskog–Fokker–Planck equation,

$$\partial_t f(\boldsymbol{v}) - \frac{\partial}{\partial \boldsymbol{v}}\cdot\left[\zeta(v)\boldsymbol{v} + \frac{\xi^2(v)}{2}\frac{\partial}{\partial \boldsymbol{v}}\right] f(\boldsymbol{v}) = J[\boldsymbol{v}|f,f]. \tag{2.1}$$

On the one hand, the force exerted by the background fluid on the Brownian particles has two components: a nonlinear drag force $\boldsymbol{F}_{\text{drag}} = -m\zeta(v)\boldsymbol{v}$ and a white-noise stochastic force with nonlinear variance $m^2\xi^2(v)$. On the other hand, collisions between Brownian particles are accounted for by the Boltzmann–Enskog collision operator,[41,42]

$$J[\boldsymbol{v}_1|f,f] = \sigma^{d-1} g(\sigma)\int d\boldsymbol{v}_2 \int d\widehat{\boldsymbol{\sigma}}\,\Theta(\boldsymbol{v}_{12}\cdot\widehat{\boldsymbol{\sigma}})\boldsymbol{v}_{12}\cdot\widehat{\boldsymbol{\sigma}} \times [f(\boldsymbol{v}_1')f(\boldsymbol{v}_2') - f(\boldsymbol{v}_1)f(\boldsymbol{v}_2)]. \tag{2.2}$$

Therein, $g(\sigma) = \lim_{r\to\sigma^+} g(r)$ is the contact value of the pair correlation function $g(r)$, $\Theta(\cdot)$ is the Heaviside step function, $\boldsymbol{v}_{12} \equiv \boldsymbol{v}_1 - \boldsymbol{v}_2$ is the relative velocity, and

$$\boldsymbol{v}_1' = \boldsymbol{v}_1 - (\boldsymbol{v}_{12}\cdot\widehat{\boldsymbol{\sigma}})\widehat{\boldsymbol{\sigma}}, \quad \boldsymbol{v}_2' = \boldsymbol{v}_2 + (\boldsymbol{v}_{12}\cdot\widehat{\boldsymbol{\sigma}})\widehat{\boldsymbol{\sigma}} \tag{2.3}$$

are the postcollisional velocities. Note that in the spatially uniform states under consideration, the Enskog collision operator (2.2) is simply Boltzmann's multiplied by the factor $g(\sigma)$.

The velocity-dependent coefficients $\zeta(v)$ and $\xi(v)$ are related by the condition that Eq. (2.1) admits as a stationary solution the equilibrium VDF,

$$f_{\text{s}}(\boldsymbol{v}) = n\left(\frac{m}{2\pi k_B T_{\text{s}}}\right)^{d/2} e^{-mv^2/2k_B T_{\text{s}}}, \tag{2.4}$$

where $k_B$ is the Boltzmann constant and $T_{\text{s}}$ is the equilibrium temperature of the background fluid, which acts as a thermostat. This yields the fluctuation–dissipation relation,

$$\xi^2(v) = \frac{2k_B T_{\text{s}}}{m}\zeta(v). \tag{2.5}$$

Equation (2.1) can then be rewritten as

$$\partial_t f(\boldsymbol{v}) - \frac{\partial}{\partial \boldsymbol{v}}\cdot\zeta(v)\left(\boldsymbol{v} + \frac{k_B T_{\text{s}}}{m}\frac{\partial}{\partial \boldsymbol{v}}\right) f(\boldsymbol{v}) = J[\boldsymbol{v}|f,f], \tag{2.6}$$

which describes the Brownian motion of an ensemble of particles of mass $m$ moving in the background fluid. These Brownian particles are not independent, with their interaction being incorporated through the collision term.

In this work, as the simplest nonlinear model, we consider the quadratic dependence of the drag coefficient on the velocity derived in Refs. 34–36. Thus, we restrict ourselves to

$$\zeta(v) = \zeta_0\left(1 + \gamma\frac{mv^2}{k_B T_{\text{s}}}\right), \tag{2.7}$$

where $\gamma > 0$ is a dimensionless parameter measuring the degree of nonlinearity of the drag force. When both Brownian particles and background fluid particles are three-dimensional hard spheres, it has been shown that $\gamma = m_{\text{bf}}/10m$.[34–36] See also Appendix A. In this work, we restrict ourselves to $m_{\text{bf}} \le 2m$, i.e., $\gamma \le 0.2$.

By taking velocity moments in Eq. (2.6), the evolution equation for temperature

$$T = \frac{m}{k_B d}\langle v^2\rangle = \frac{m}{k_B n d}\int d\boldsymbol{v}\, v^2 f(\boldsymbol{v}), \tag{2.8}$$

where $n = \int d\boldsymbol{v} f(\boldsymbol{v})$ is the number density, is obtained as

$$\frac{\dot{T}}{\zeta_0} = 2(T_s - T)\left[1 + \gamma(d+2)\frac{T}{T_s}\right] - 2\gamma(d+2)\frac{T^2}{T_s}a_2, \tag{2.9}$$

in which we have introduced the excess kurtosis

$$a_2 = \frac{d}{d+2}\frac{\langle v^4\rangle}{\langle v^2\rangle^2} - 1. \tag{2.10}$$

In the particular case of a linear drag, $\gamma = 0$, the solution to Eq. (2.9) is simply $T(t) = T_s + [T(0) - T_s]e^{-2\zeta_0 t}$. However, in the case of nonlinear drag, $\gamma > 0$, the evolution of temperature is coupled to that of excess kurtosis. Imagine that $T(0) > T_s$; the larger the value of $a_2(0)$, the larger the initial cooling rate is and the sooner the temperature is expected to reach the thermostat value $T_s$. This property can give rise to an Mpemba phenomenon, as reported in the case of granular fluids.[21] Similarly, the inverse Mpemba effect, in which the cooler system heats sooner,[20,21,29] may also be expected for $T(0) < T_s$.

Since the evolution equation (2.9) involves the excess kurtosis $a_2(t)$, we need to consider its evolution equation. This in turn involves sixth-degree moments, and so on, giving rise to an infinite hierarchy of moment equations. To derive this hierarchy, let us introduce the dimensionless VDF $\phi(\boldsymbol{c})$ as

$$f(\boldsymbol{v}) = \frac{n}{v_T^d(t)}\phi(\boldsymbol{c}), \quad \boldsymbol{c} \equiv \frac{\boldsymbol{v}}{v_T(t)}, \tag{2.11}$$

where $v_T(t) \equiv \sqrt{2k_BT(t)/m}$ is the thermal velocity. Then, the kinetic equation (2.6) becomes

$$\partial_t\phi(\boldsymbol{c}) - \frac{\partial}{\partial\boldsymbol{c}}\cdot\left[\frac{\dot{T}}{2T}\boldsymbol{c} + \zeta_0\left(1 + \gamma\frac{2T}{T_s}c^2\right)\times\left(\boldsymbol{c} + \frac{T_s}{2T}\frac{\partial}{\partial\boldsymbol{c}}\right)\right]\phi(\boldsymbol{c}) = \nu_s\sqrt{\frac{T}{T_s}}I[\boldsymbol{c}|\phi,\phi], \tag{2.12}$$

in which we have defined $\nu_s \equiv g(\sigma)n\sigma^{d-1}\sqrt{2k_BT_s/m}$, which is basically the collision frequency at the steady state, and the dimensionless collision operator

$$I[\boldsymbol{c}_1|\phi,\phi] = \int d\boldsymbol{c}_2\int d\widehat{\boldsymbol{\sigma}}\,\Theta(\boldsymbol{c}_{12}\cdot\widehat{\boldsymbol{\sigma}})\,\boldsymbol{c}_{12}\cdot\widehat{\boldsymbol{\sigma}} \times[\phi(\boldsymbol{c}_1')\phi(\boldsymbol{c}_2') - \phi(\boldsymbol{c}_1)\phi(\boldsymbol{c}_2)]. \tag{2.13}$$

In addition, we have employed the property

$$\frac{v_T^d}{n}\partial_t f(\boldsymbol{v}) = \partial_t\phi(\boldsymbol{c}) - \frac{\dot{T}}{2T}\frac{\partial}{\partial\boldsymbol{c}}\cdot[\boldsymbol{c}\phi(\boldsymbol{c})]. \tag{2.14}$$

Multiplying both sides of Eq. (2.12) by $c^\ell$, integrating over $\boldsymbol{c}$, and making use of Eq. (2.9), we obtain the hierarchy of equations for the moments $M_\ell \equiv \langle c^\ell\rangle$,

$$\dot{M}_\ell = \ell\zeta_0\left\{\left[\gamma(\ell-2) + \gamma(d+2)\frac{T}{T_s}(1+a_2) - \frac{T_s}{T}\right]M_\ell - \gamma\frac{2T}{T_s}M_{\ell+2} + \frac{\ell+d-2}{2}\frac{T_s}{T}M_{\ell-2}\right\} - \nu_s\sqrt{\frac{T}{T_s}}\mu_\ell. \tag{2.15}$$

Here, we have introduced the collisional moments $\mu_\ell$ as

$$\mu_\ell \equiv -\int d\boldsymbol{c}\, c^\ell I[\boldsymbol{c}|\phi,\phi]. \tag{2.16}$$

Since, by definition, $M_0 = 1$, $M_2 = d/2$, and $M_4 = d(d+2)(1+a_2)/4$ [see Eqs. (2.8) and (2.10)], it is easy to check that, as it should be, $\dot{M}_0 = \dot{M}_2 = 0$ (note that $\mu_0 = \mu_2 = 0$). Next, setting $\ell = 4$ in Eq. (2.15), we get

$$\dot{a}_2 = \zeta_0\gamma\frac{4T}{T_s}\left[\frac{2T_s}{T}(1+a_2) + (d+2)(1+a_2)^2 - (d+4) \times(1 + 3a_2 - a_3)\right] - \zeta_0\frac{4T_s}{T}a_2 - \frac{4\nu_s}{d(d+2)}\sqrt{\frac{T}{T_s}}\mu_4, \tag{2.17}$$

where we have introduced the sixth-degree cumulant $a_3$ by

$$M_6 = \frac{d(d+2)(d+4)}{8}(1 + 3a_2 - a_3). \tag{2.18}$$

Some comments are in order. First, note that two time scales compete in Eqs. (2.15) and (2.17). The inverse of the drag coefficient for low velocities, $\zeta_0^{-1}$, dictates the time scale over which particles feel the action of the background fluid. Meanwhile, the characteristic time for particle–particle collisions is the inverse of the stationary collision frequency, $\nu_s^{-1}$. Second, Eqs. (2.9), (2.15), and (2.17) are formally exact within the Enskog–Fokker–Planck description, but they do not make a closed finite set. Not only does $\dot{M}_\ell$ explicitly involve a higher-degree moment $M_{\ell+2}$ but also the collisional moment $\mu_\ell$ is a nonlinear functional of the full VDF $\phi(\boldsymbol{c})$. An approximate closure is needed to deal with a finite set of equations.

## III. SONINE APPROXIMATION

For isotropic states, the reduced VDF $\phi(\boldsymbol{c})$ can be expanded in a complete set of orthogonal polynomials as

$$\phi(\boldsymbol{c}) = \frac{e^{-c^2}}{\pi^{d/2}}\left[1 + \sum_{\ell=2}^{\infty}a_\ell L_\ell^{\left(\frac{d-2}{2}\right)}(c^2)\right], \tag{3.1}$$

where $L_\ell^{(\alpha)}(x)$ is a generalized Laguerre (or Sonine) polynomial.[43] Of course, the coefficients with $\ell = 2$ and $\ell = 3$ in Eq. (3.1) are the same as the cumulants $a_2$ and $a_3$, respectively, introduced before [see Eqs. (2.10) and (2.18)].

In the first Sonine approximation, all terms beyond $\ell = 2$ in Eq. (3.1) are dropped, i.e.,

$$\phi(\boldsymbol{c}) \approx \frac{e^{-c^2}}{\pi^{d/2}}\left\{1 + a_2\left[\frac{c^4}{2} - \frac{d+2}{2}c^2 + \frac{d(d+2)}{8}\right]\right\}. \tag{3.2}$$

Inserting Eq. (3.2) into Eq. (2.16) with $\ell = 2$ and neglecting terms quadratic in $a_2$, one obtains $\Gamma(d/2)\mu_4 \approx \sqrt{2}(d-1)\pi^{\frac{d-1}{2}}a_2$.[44–46] Therefore, Eq. (2.17) becomes

$$\dot{a}_2 = 8\zeta_0\gamma\left(1 - \frac{T}{T_s}\right) - \left\{\zeta_0\left[\frac{4T_s}{T} - 8\gamma + 4\gamma(d+8)\frac{T}{T_s}\right] + \tau_s^{-1}\frac{8(d-1)}{d(d+2)}\sqrt{\frac{T}{T_s}}\right\}a_2, \tag{3.3}$$

where we have introduced the mean free time at the steady state[47,48]

$$\tau_s = \sqrt{2}\,\Gamma(d/2)\pi^{\frac{1-d}{2}} v_s^{-1}, \tag{3.4}$$

and, for consistency, the terms $a_2^2$ and $a_3$ have been neglected.

Equations (2.9) and (3.3) make a closed set to investigate the existence of the Mpemba effect. First, we define dimensionless temperature and time by

$$\theta \equiv \frac{T}{T_s}, \qquad t^* \equiv \frac{t}{\tau_s}. \tag{3.5}$$

The latter approximately measures the accumulated number of collisions per particle up to time $t$. With these variables, Eqs. (2.9) and (3.3) can be rewritten as

$$\frac{\dot{\theta}}{\zeta_0^*} = 2(1-\theta)[1+\gamma(d+2)\theta] - 2\gamma(d+2)\theta^2 a_2, \tag{3.6a}$$

$$\frac{\dot{a}_2}{\zeta_0^*} = 8\gamma(1-\theta) - \left[\frac{4}{\theta} - 8\gamma + 4\gamma(d+8)\theta + \frac{8(d-1)}{d(d+2)}\frac{\sqrt{\theta}}{\zeta_0^*}\right]a_2, \tag{3.6b}$$

where we have introduced a dimensionless low-velocity drag coefficient as

$$\zeta_0^* \equiv \zeta_0 \tau_s. \tag{3.7}$$

Now, the dot over $\theta$ and $a_2$ denotes a derivative with respect to $t^*$.

Equations (3.6) are linear in the excess kurtosis $a_2$ but nonlinear in the temperature ratio $\theta$. They constitute our starting point for the analysis of the Mpemba effect, to be carried out in Sec. IV. In the dimensionless variables we are using, there are only two relevant parameters: (i) $\gamma$, which measures the strength of the nonlinearity in the drag, and (ii) $\zeta_0^*$, which compares the characteristic times for collisions, $\tau_s$, and for the viscous drag, $\zeta_0^{-1}$. Note that the regime $\zeta_0^* \ll 1$ ($\zeta_0^* \gg 1$) means that the viscous drag acts over a much longer (shorter) time scale than collisions do.

## IV. MPEMBA EFFECT

### A. Linearized model

Let us imagine two initial states A and B with $\{\theta(0), a_2(0)\} = \{\theta_A^0, a_{2A}^0\}$ and $\{\theta_B^0, a_{2B}^0\}$, respectively. The corresponding solutions to Eq. (3.6) are denoted by $\{\theta_A(t^*), a_{2A}(t^*)\}$ and $\{\theta_B(t^*), a_{2B}(t^*)\}$. Without loss of generality, we assume that $\theta_A^0 > \theta_B^0$.[49]

Now, we show that both the Mpemba effect and its inverse version are expected to emerge when the initially hotter sample has a larger value of the excess kurtosis. First, we analyze the case in which both initial temperatures are higher than the stationary one, $\theta_A^0 > \theta_B^0 > 1$, and the system cools down to reach the steady state. The Mpemba effect is present when $\theta_A(t^*)$ relaxes more rapidly than $\theta_B(t^*)$, which calls for the existence of a crossover time $t_c^*$ such that $\theta_A(t_c^*) = \theta_B(t_c^*)$. Since the cooling rate increases with $a_2$, the condition $a_{2A}^0 > a_{2B}^0$ seems to be necessary for the Mpemba effect to emerge. Second, we look into the case in which both temperatures are lower than the stationary value, $1 > \theta_A^0 > \theta_B^0$, and the system heats up. The inverse Mpemba effect appears if $\theta_A(t^*)$ relaxes more slowly than $\theta_B(t^*)$, which again needs $a_{2A}^0 > a_{2B}^0$.

In general, the nonlinear dependence on $\theta$ of the set of Eq. (3.6) impedes a fully analytical treatment. However, the excess kurtosis is supposed to be small in the Sonine approximation, which has allowed us to neglect nonlinear terms in $a_2$. Since $a_2$ is the quantity controlling the appearance of the Mpemba effect, its smallness implies that both initial temperatures, $\theta_A^0$ and $\theta_B^0$, cannot be very far from each other for the Mpemba effect to emerge. In addition, the crossing of the curves $\theta_A(t^*)$ and $\theta_B(t^*)$ must take place at the early stage of evolution.[50]

Following the discussion above, we write $\theta(t^*) = \theta_r + \Psi(t^*)$, where $\theta_r \approx \theta_A^0 \approx \theta_B^0$ is a certain *reference* temperature, and linearize Eq. (3.6) with respect to $\Psi(t^*)$ and $a_2(t^*)$. The detailed solution of this linearization procedure is carried out in Appendix B; here, we present the results relevant for the analysis of the Mpemba effect. The time evolution is controlled by the matrix $\Lambda$ with elements

$$\Lambda_{11} = 2\zeta_0^*[1+\gamma(d+2)(2\theta_r - 1)], \tag{4.1a}$$

$$\Lambda_{12} = 2\zeta_0^*\gamma(d+2)\theta_r^2, \tag{4.1b}$$

$$\Lambda_{21} = 8\zeta_0^*\gamma, \tag{4.1c}$$

$$\Lambda_{22} = \zeta_0^*\left[\frac{4}{\theta_r} - 8\gamma + 4\gamma(d+8)\theta_r\right] + \frac{8(d-1)}{d(d+2)}\sqrt{\theta_r}, \tag{4.1d}$$

and eigenvalues

$$\lambda_\pm = \frac{\Lambda_{11} + \Lambda_{22} \pm \delta_\lambda}{2}, \quad \delta_\lambda \equiv \sqrt{(\Lambda_{11} - \Lambda_{22})^2 + 4\Lambda_{12}\Lambda_{21}}. \tag{4.2}$$

Let us consider the differences $\Delta\theta(t^*) \equiv \theta_A(t^*) - \theta_B(t^*)$ and $\Delta a_2(t^*) \equiv a_{2A}(t^*) - a_{2B}(t^*)$ between the time evolutions corresponding to the two different initial states A and B. Within the linearized theory, these differences are given by (see Appendix B)

$$\Delta\theta(t^*) = \left(\frac{\lambda_+ - \Lambda_{11}}{\delta_\lambda}\Delta\theta^0 - \frac{\Lambda_{12}}{\delta_\lambda}\Delta a_2^0\right)e^{-\lambda_- t^*} - \left(\frac{\lambda_- - \Lambda_{11}}{\delta_\lambda}\Delta\theta^0 - \frac{\Lambda_{12}}{\delta_\lambda}\Delta a_2^0\right)e^{-\lambda_+ t^*}, \tag{4.3a}$$

$$\Delta a_2(t^*) = \left(\frac{\lambda_+ - \Lambda_{22}}{\delta_\lambda}\Delta a_2^0 - \frac{\Lambda_{21}}{\delta_\lambda}\Delta\theta^0\right)e^{-\lambda_- t^*} - \left(\frac{\lambda_- - \Lambda_{22}}{\delta_\lambda}\Delta a_2^0 - \frac{\Lambda_{21}}{\delta_\lambda}\Delta\theta^0\right)e^{-\lambda_+ t^*}. \tag{4.3b}$$

Note that both $\Delta\theta$ and $\Delta a_2$ vanish in the long-time limit.

### B. Mpemba crossover

The accuracy of the linearized theory developed above for describing the Mpemba effect—and the inverse Mpemba effect—is illustrated in Fig. 1. The linear theory remains valid even when the system is initially far from the steady state; the analytical expressions of the linearized theory, given by Eq. (B4), predict the crossover of the curves correctly but start to deviate from the "exact" numerical integration as time grows. For all these plots, an optimal choice for $\theta_r$ is the initial temperature of the sample that is closer to the

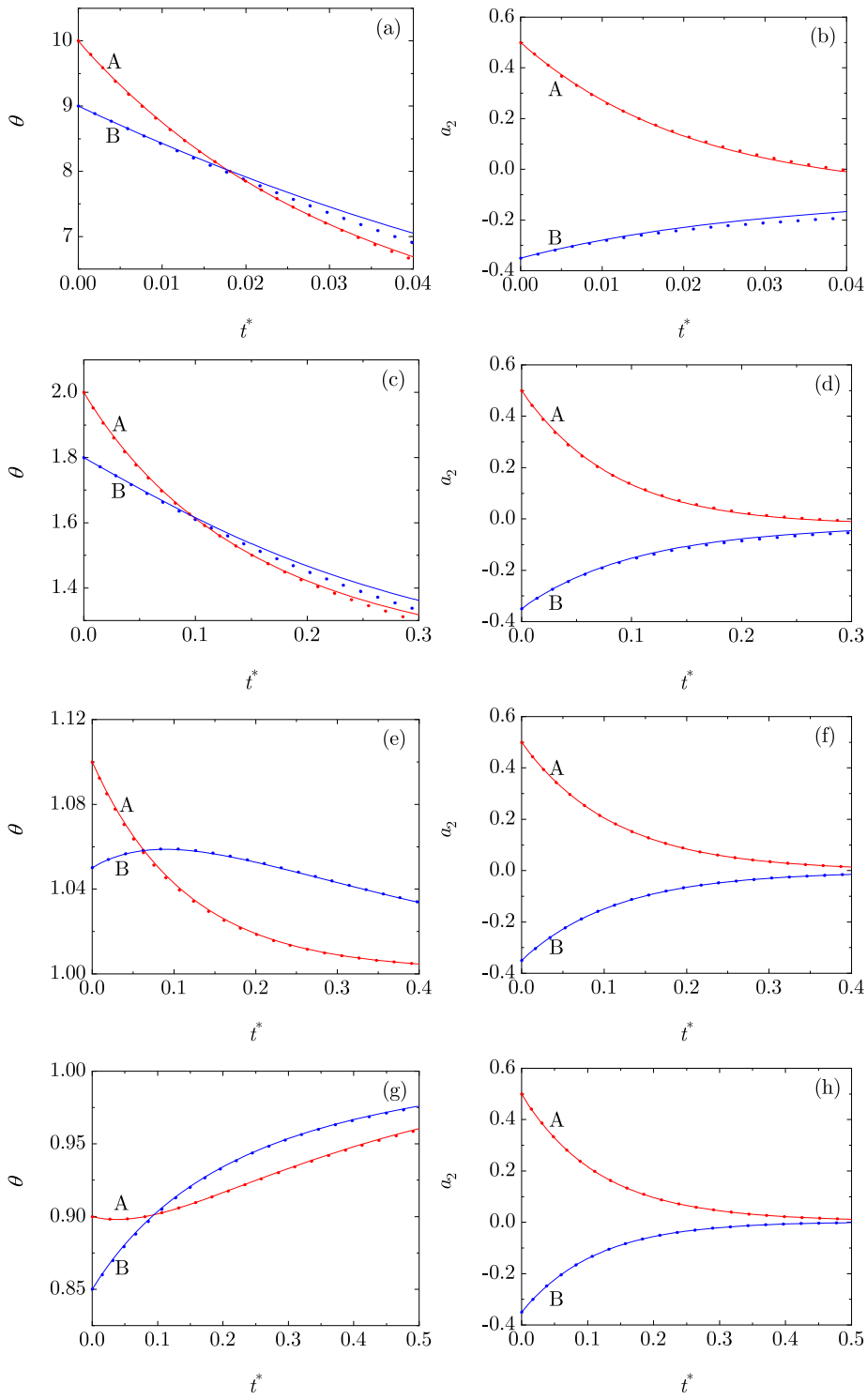


**FIG. 1**. First stage in the evolution of $\theta_A(t^*)$ and $\theta_B(t^*)$ [panels (a), (c), (e), and (g)] and $a_{2A}(t^*)$ and $a_{2B}(t^*)$ [panels (b), (d), (f), and (h)] for $d = 3$, $\zeta_0^* = 1$, and $\gamma = 0.1$. The initial states are $a_{2A}^0 = 0.5$, $a_{2B}^0 = -0.35$, and [(a) and (b)] $\theta_A^0 = 10$, $\theta_B^0 = 9$, [(c) and (d)] $\theta_A^0 = 2$, $\theta_B^0 = 1.8$, [(e) and (f)] $\theta_A^0 = 1.1$, $\theta_B^0 = 1.05$, and [(g) and (h)] $\theta_A^0 = 0.9$, $\theta_B^0 = 0.85$. Circles correspond to the numerical solutions of Eq. (3.6), whereas solid lines correspond to the linearized model, given by Eq. (B4). The Mpemba effect is neatly observed in panels (a), (c), and (e). The linearized theory with $\theta_r = \theta_B^0$ gives a correct account thereof—although it deviates from the numerical solution of Eq. (3.6) as time increases in panels (a) and (c), for which their initial temperatures are not close to the steady value. The inverse Mpemba effect is depicted in panel (g), and the linear theory also describes it correctly, but now we have chosen $\theta_r = \theta_A^0$.

steady state. Figure 1 also shows that the excess kurtosis relaxes to equilibrium more rapidly than temperature.

Let us now restrict ourselves to a situation in which the Mpemba effect is present. Thus, there exists a crossover time such that $\Delta\theta(t_c^*) = 0$. According to Eq. (4.3a), it is given by

$$t_c^* = \frac{1}{\delta_\lambda} \ln \frac{\Lambda_{12} - (\lambda_- - \Lambda_{11})R^0}{\Lambda_{12} - (\lambda_+ - \Lambda_{11})R^0}, \quad R^0 \equiv \frac{\Delta\theta^0}{\Delta a_2^0}. \tag{4.4}$$

The crossover time $t_c^*$ depends on the initial preparation *only* through the reference temperature $\theta_r \approx \theta_A^0 \approx \theta_B^0$ and the ratio $R^0$ in this simplified description, for given values of $\zeta_0^*$ and $\gamma$. Note that we have chosen $\Delta\theta^0 > 0$ and, for the Mpemba effect to exist, we need that $\Delta a_2^0 > 0$, i.e., we have that $R^0 > 0$.

Figure 2 displays $t_c^*$ as a function of $R^0$ for some illustrative cases. Different panels correspond to different values of the reference temperature. In all of them, the crossover time $t_c^*$ vanishes in the limit as $R^0 \to 0$ and grows with $R^0$. Figure 2 also includes the values of the crossover time obtained from the numerical solution of Eq. (3.6) for $a_{2A}^0 = 0.5$ and $a_{2B}^0 = -0.35$ with $\theta_B^0 = \theta_r$ in panels (a)–(c) and $\theta_A^0 = \theta_r$ in panel (d). It is observed that the agreement with Eq. (4.4) improves as $\gamma$ increases and $R^0$ decreases. In addition, Eq. (4.4) underestimates the crossover time for the direct Mpemba effect with initial temperatures far from that of the thermostat, while it tends to overestimate $t_c^*$ for the inverse Mpemba effect or when the initial temperatures are close to the thermostat one.

Equation (4.4) shows that $t_c^*$ diverges in the limit as $R^0 \to R_{\text{th}}^0$, where $R_{\text{th}}^0$ is a *threshold* value for the ratio, given by

$$R_{\text{th}}^0 = \frac{\Lambda_{12}}{\lambda_+ - \Lambda_{11}}. \tag{4.5}$$

Thus, the Mpemba effect disappears if $R^0 \geq R_{\text{th}}^0$: in this region, $t_c^*$, as defined by Eq. (4.4), ceases to be a real number. In fact, if we define

$$\beta \equiv \frac{\lambda_- - \Lambda_{11}}{\lambda_+ - \Lambda_{11}} = 1 - \frac{\delta_\lambda}{\lambda_+ - \Lambda_{11}}, \tag{4.6}$$

we can rewrite $t_c^*$ as

$$t_c^* = \frac{1}{\delta_\lambda} \ln \frac{1 - \beta R^0/R_{\text{th}}^0}{1 - R^0/R_{\text{th}}^0}. \tag{4.7}$$

The emergence of the Mpemba effect is basically controlled by the strength of the drag nonlinearity $\gamma$. As expected on a physical basis, the Mpemba crossover takes place earlier as $\gamma$ increases. Throughout Fig. 2, the curves for $\gamma = 0.1$ lie above those for $\gamma = 0.2$. Thus, the smaller $\gamma$ is, the smaller the threshold value $R_{\text{th}}^0$ we find. Recall that the drag becomes linear in the limit as $\gamma \to 0^+$, for which the temperature obeys a closed first-order differential equation, independent of the value of the excess kurtosis, and the Mpemba effect is no longer present. Note also that terms beyond the quadratic one in the expansion of $\zeta(v)$ in powers of $v$ might be necessary as $\gamma$ (or, equivalently, $m_{\text{bf}}/m$) increases.

### C. Phase diagram

A phase diagram in the $(\gamma, R^0)$ plane can be constructed, as illustrated in Fig. 3. The line $R^0 = R_{\text{th}}^0$ separates the regions in which the Mpemba effect is present ($R^0 < R_{\text{th}}^0$) and absent ($R^0 > R_{\text{th}}^0$), where $R_{\text{th}}^0$ is defined in Eq. (4.5). The range $0 < R^0 < R_{\text{th}}^0$ for which the Mpemba effect emerges increases with $\gamma$, $\zeta_0^*$, and $\theta_r$. It must be remarked that $\theta_r < 1$ corresponds to the inverse Mpemba effect, in which the system relaxes to equilibrium from below the steady temperature $T_s$.

The threshold values $R_{\text{th}}^0$ obtained from the numerical solution of Eq. (3.6) for $a_{2A}^0 = 0.5$ and $a_{2B}^0 = -0.35$ are also shown in Fig. 3.

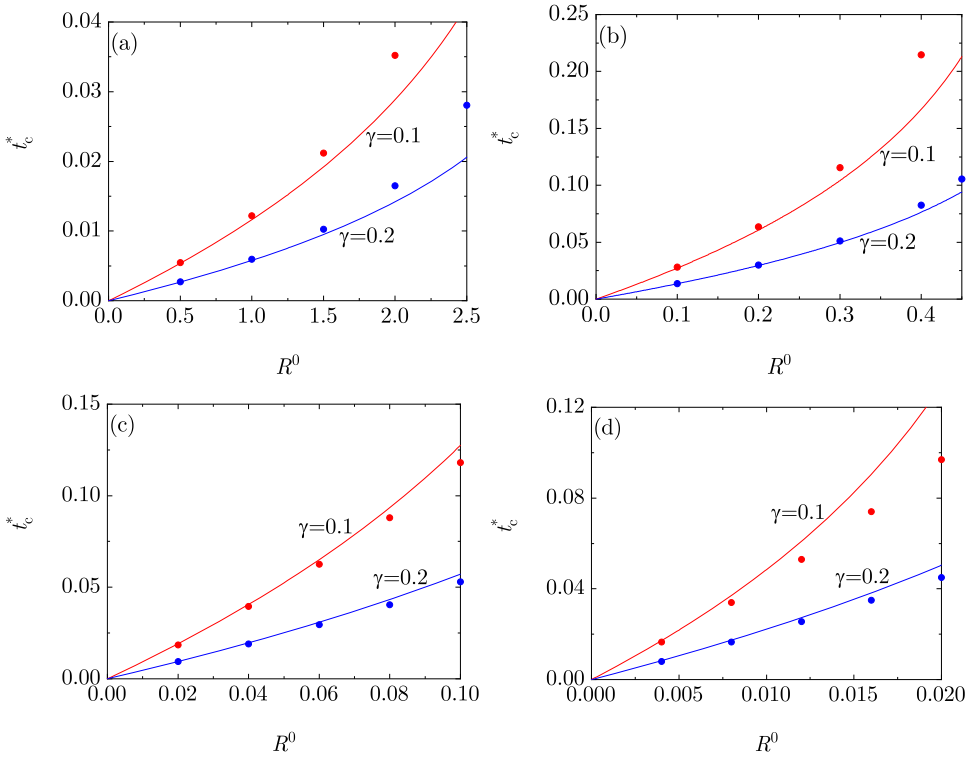


**FIG. 2.** Crossover time $t_c^*$ as a function of $R^0 \equiv \Delta\theta^0/\Delta a_2^0$ [see Eq. (4.4)]. All the panels correspond to $d = 3$ and $\zeta_0^* = 1$, but to different values of the reference temperature: $\theta_r = 10$, 2, 1.05, and 0.5, from (a) to (d). In each panel, two values of the nonlinearity parameter are considered: $\gamma = 0.1$ (upper curves) and 0.2 (lower curves). The crossover time decreases as the nonlinearity coefficient $\gamma$ increases, as expected. The symbols are the values obtained from the numerical solution of Eq. (3.6) with $a_{2A}^0 = 0.5$ and $a_{2B}^0 = -0.35$.

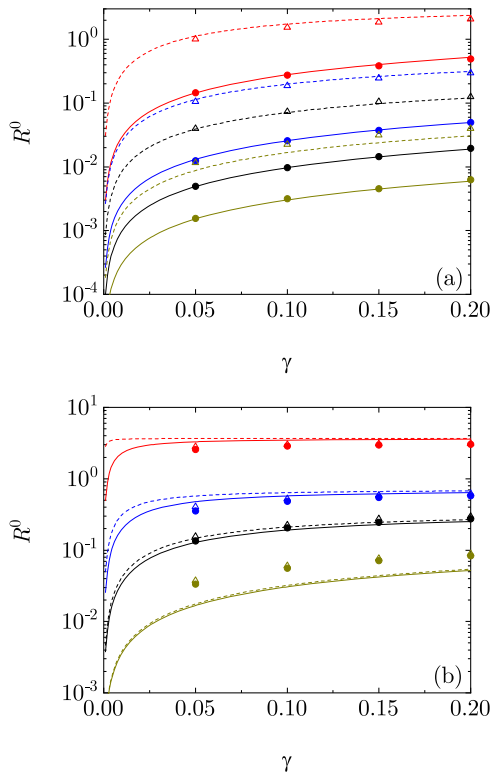


**FIG. 3**. Phase diagram in the plane $R^0 \equiv \Delta\theta^0/\Delta a_2^0$ vs $\gamma$ for $d = 3$. The values of $\zeta_0^*$ are (a) $\zeta_0^* = 0.01$ (solid curves and closed circles) and 0.1 (dashed curves and open triangles) and (b) $\zeta_0^* = 1$ (solid curves and closed circles) and 2 (dashed curves and open triangles). From the bottom to the top in each panel, $\theta_r = 0.5$, 1.05, 2, and 10. In each case, the Mpemba effect is present (absent) below (above) the corresponding curve. Symbols are obtained by numerically solving Eq. (3.6) with $a_{2A}^0 = 0.5$ and $a_{2B}^0 = -0.35$, whereas lines correspond to the analytical prediction given by Eq. (4.5).

The agreement with the simplified model is quite good, especially in panel (a), for which $\zeta_0^* < 1$. In panel (b), for which $\zeta_0^* \geq 1$, the linearized theory still gives a semi-quantitative picture and, notably, successfully captures the weak influence of both $\gamma$ and $\zeta_0^*$ on $R_{\text{th}}^0$ if $\zeta_0^* \geq 1$. In any case, the linear model overestimates (underestimates) $R_{\text{th}}^0$ for $\theta_r = 10$ and 2 ($\theta_r = 1.05$ and 0.5), as anticipated from Fig. 2.

Interestingly, the maximum ratio *relative* to the reference temperature, $\theta_r^{-1} R_{\text{th}}^0$, keeps increasing with increasing $\theta_r$. At fixed $\theta_r$, the upper bound of $R_{\text{th}}^0$ corresponds to the limit $\gamma \to \infty$, which is independent of $\zeta_0^*$, namely,

$$\lim_{\gamma\to\infty} R_{\text{th}}^0 = \frac{2(d+2)\theta_r^2/(d-2+12\theta_r)}{1+\sqrt{1+16(d+2)\theta_r^2/(d-2+12\theta_r)^2}}. \tag{4.8}$$

Notwithstanding, in our modeling, we are only retaining the first correction, quadratic in the velocities, in the drag coefficient $\zeta(v)$. Therefore, from a physical point of view, $\gamma$ is expected not to be very large; otherwise, higher order terms in the velocity should be incorporated into the drag coefficient.

## D. Magnitude of the Mpemba effect

When the Mpemba effect is present, the temperature difference $\Delta\theta$ vanishes at the crossover time $t_c^*$. Since $\Delta\theta$ also vanishes in the long time limit as $t^* \to \infty$, there must exist a certain time $t_m^* > t_c^*$ where $|\Delta\theta(t^*)|$ reaches a local maximum. Therefore, one has that $|\Delta\theta(t^*)| \leq |\Delta\theta(t_m^*)|$ for any time $t^* > t_c^*$.

The above discussion can be used to introduce a quantitative measure of the magnitude of the Mpemba effect. Let us define[28]

$$\text{Mp} \equiv |\Delta\theta(t_m^*)| \tag{4.9}$$

as a quantitative measure of its magnitude. From Eq. (4.3), one finds

$$t_m^* = t_c^* + \frac{1}{\delta_\lambda} \ln \frac{\lambda_+}{\lambda_-}, \tag{4.10a}$$

$$\frac{\text{Mp}}{\Delta a_2^0} = \Lambda_{12} \left(\frac{1-R^0/R_{\text{th}}^0}{\lambda_+}\right)^{\frac{\lambda_+}{\delta_\lambda}} \left(\frac{\lambda_-}{1-\beta R^0/R_{\text{th}}^0}\right)^{\frac{\lambda_-}{\delta_\lambda}}. \tag{4.10b}$$

Thus, the Mpemba magnitude Mp depends on the initial differences $\Delta\theta^0$ and $\Delta a_2^0$ by a simple scaling law: the ratio $\text{Mp}/\Delta a_2^0$ is a function of the ratio $R^0 \equiv \Delta\theta^0/\Delta a_2^0$. Figure 4 shows that the larger the ratio $R^0$ is, the smaller $\text{Mp}/\Delta a_2^0$ becomes. Of course, Mp vanishes as $R^0$ approaches its threshold value $R_{\text{th}}^0$, as readily seen in Eq. (4.10b). Comparison with the values of Mp obtained from the numerical solution of Eq. (3.6) shows that the simple linearized model is qualitatively correct in capturing the dependence of the order of magnitude of Mp on the parameters of the problem. In agreement with what was observed in Figs. 2 and 3, the linearized model tends to overestimate (underestimate) Mp for the direct (inverse) Mpemba effect. Figure 4(c) shows that the prediction of Mp is especially accurate if the initial temperatures are close to the equilibrium one; in that case, Mp is slightly overestimated for small $R^0$, while it is slightly underestimated as $R^0$ approaches its threshold value $R_{\text{th}}^0$.

## E. Reliability of the linear theory

The linear theory we have presented does not apply for all times, unless the reference temperature $\theta_r = \theta_s = 1$ and both initial temperatures $\theta_A^0$ and $\theta_B^0$ are close to the steady state. Nevertheless, as already stated before, our linear theory is not the standard linearization around the steady state but an approximate scheme to obtain a good approximation to the actual time evolution of the system at the early stage of its evolution, where the Mpemba effect is expected to come about. This means that our linear approach does have some limitations, as observed in Figs. 2–4. According to them, the linearized model becomes more accurate as $|\theta_r - 1|$ and $\zeta_0^*$ decrease.

While a complete account of the range of validity of the linear approximation is outside the scope of our paper, quite simple arguments can be presented in the limit of weak nonlinearity, $\gamma \to 0^+$. The behavior of the threshold $R_{\text{th}}^0$—below which the Mpemba effect is found—depends on that of its numerator, $\Lambda_{12}$, and its denominator, $\lambda_+ - \Lambda_{11}$. On the one hand, Eq. (4.1b) tells us that the former is linear in $\gamma$, $\Lambda_{12} = O(\gamma)$. On the other hand, the behavior of $\lambda_+ - \Lambda_{11}$ for small $\gamma$ depends on the sign of the function

$$\varphi(\theta_r, \zeta_0^*) \equiv \frac{4(d-1)}{d(d+2)\zeta_0^*} \theta_r^{3/2} - \theta_r + 2. \tag{4.11}$$

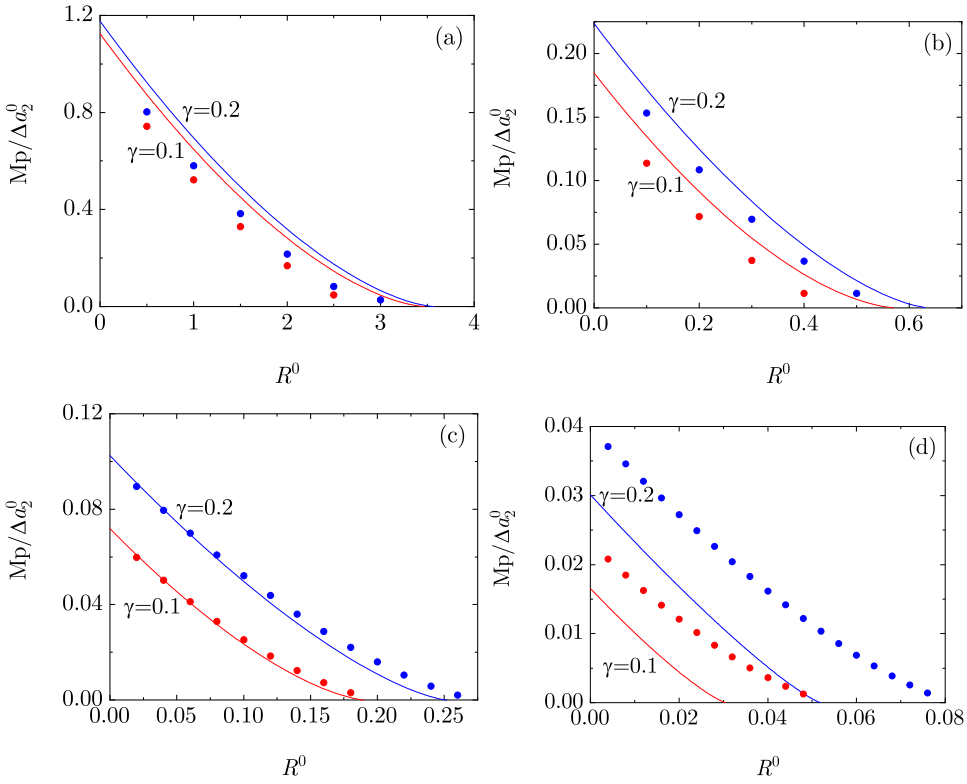


**FIG. 4**. Magnitude of the Mpemba effect, $\mathrm{Mp}/\Delta a_2^0$, as a function of $R^0 \equiv \Delta\theta^0/\Delta a_2^0$. The parameter values are the same as that given in Fig. 2: (i) in all the panels, we have that $d = 3$ and $\zeta_0^* = 1$ and (ii) from panel (a) to (d), different values of the reference temperature are considered, namely, $\theta_r = 10$, 2, 1.05, and 0.5, with two values of the nonlinearity parameter being considered in each panel, $\gamma = 0.1$ (lower curves) and 0.2 (upper curves). Again, symbols are obtained by numerically solving Eq. (3.6) with $a_{2A}^0 = 0.5$ and $a_{2B}^0 = -0.35$, whereas lines correspond to the analytical prediction given by Eq. (4.10b).

Specifically, it can be readily shown that

$$\lambda_+ - \Lambda_{11} \approx \begin{cases} \dfrac{2\zeta_0^*\varphi(\theta_r,\zeta_0^*)}{\theta_r}, & \varphi(\theta_r,\zeta_0^*) > 0 \\ -\dfrac{8\zeta_0^*(d+2)\theta_r^3}{\varphi(\theta_r,\zeta_0^*)}\gamma^2, & \varphi(\theta_r,\zeta_0^*) < 0, \end{cases} \tag{4.12}$$

and thus,

$$R_{\mathrm{th}}^0 \sim \begin{cases} (d+2)\theta_r^3\dfrac{\gamma}{\varphi(\theta_r,\zeta_0^*)}, & \varphi(\theta_r,\zeta_0^*) > 0 \\ -\dfrac{1}{4\theta_r}\dfrac{\varphi(\theta_r,\zeta_0^*)}{\gamma}, & \varphi(\theta_r,\zeta_0^*) < 0. \end{cases} \tag{4.13}$$

In the limit as $\gamma \to 0^+$, the drag becomes linear, the temperature obeys a closed equation, and no Mpemba effect can be present in the system. This is consistent with the behavior found for the threshold $R_{\mathrm{th}}^0$ when $\varphi(\theta_r,\zeta_0^*) > 0$; therein, $R_{\mathrm{th}}^0 \to 0$. However, $R_{\mathrm{th}}^0 \to \infty$ when $\varphi(\theta_r,\zeta_0^*) < 0$; this is an unphysical result that makes us conclude that the simplified linear model (4.3) ceases to be reliable if $\varphi(\theta_r,\zeta_0^*) < 0$ and $\gamma \ll 1$. The locus $\varphi(\theta_r,\zeta_0^*) = 0$ is plotted in Fig. 5.

The above discussion should not be employed to disregard the linear model directly when $\varphi(\theta_r,\zeta_0^*) < 0$; the linearization can be useful unless $\gamma$ is very small. We can estimate the value of $\gamma$ for which the linear theory is no longer accurate by asking the estimate for $R_{\mathrm{th}}^0$ in (4.13) to be large. This leads to the condition

$$\gamma \ll \gamma_\ell \equiv \frac{|\varphi(\theta_r,\zeta_0^*)|}{4\theta_r}. \tag{4.14}$$

We illustrate the above result in Fig. 6 for the three-dimensional case, specifically for $\zeta_0^* = 5$ and $\theta_r = 9$, in which case we have $\varphi(\theta_r,\zeta_0^*) \simeq -4.12$ and $\gamma_\ell \simeq 0.114$. While the (weak) Mpemba effect predicted by the linearized model with $\gamma = 0.001$ is actually absent,

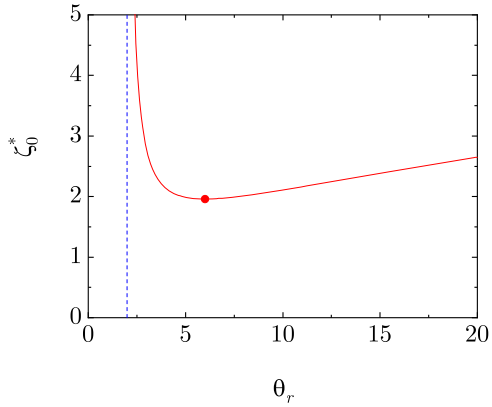


**FIG. 5**. Locus $\varphi(\theta_r,\zeta_0^*) = 0$ in the plane $\zeta_0^*$ vs $\theta_r$ for $d = 3$. The function $\varphi(\theta_r,\zeta_0^*)$, given by Eq. (4.11), is negative above (positive below) the curve. The circle represents the minimum $\theta_r = 6$, $\zeta_0^* = \frac{4}{5}\sqrt{6} \simeq 1.96$, whereas the dashed line at $\theta_r = 2$ is the vertical asymptote of the left branch of the locus. Thus, $\zeta_0^*$ must be large enough, specifically larger than its value at the minimum, to allow for negative values of $\varphi$.

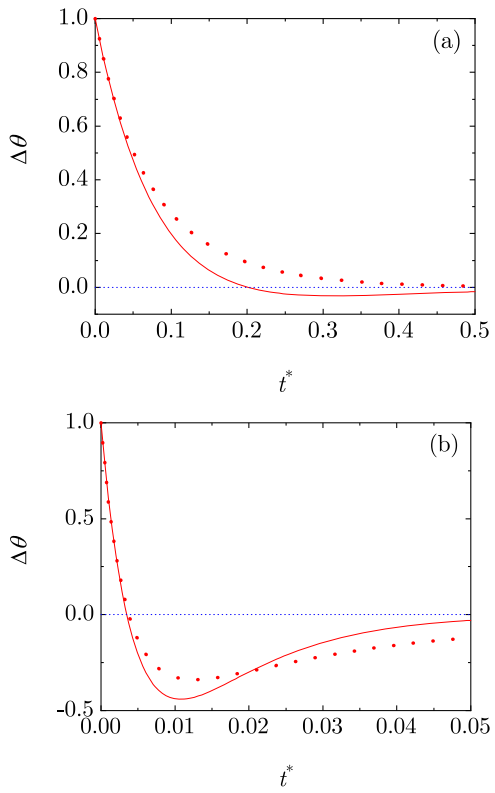


**FIG. 6.** Evolution of $\Delta\theta(t^*) = \theta_A(t^*) - \theta_B(t^*)$ for $d = 3$, $\zeta_0^* = 5$. The two panels correspond to small values of $\gamma$, namely, (a) $\gamma = 0.001$ and (b) $\gamma = 0.1$. The initial states are $\{\theta_A^0, a_{2A}^0\} = \{10, 0.5\}$ and $\{\theta_B^0, a_{2B}^0\} = \{9, -0.35\}$. Circles correspond to the numerical solutions of Eq. (3.6), whereas solid lines correspond to the linearized model (4.3) with $\theta_r = \theta_B^0$. The value of $\gamma$ in panel (a) verifies condition (4.14) that controls the failure of the linearized theory.

the model succeeds in locating the crossover time if $\gamma = 0.1$, which is quite close to $\gamma_\ell$. Note that $\gamma = 0.1$ corresponds to the case in which the mass of the Brownian particles and that of the surrounding fluid are identical, as shown in Appendix A.

## V. CONCLUSIONS

We have neatly observed the Mpemba effect in a molecular gas with nonlinear drag. For the Mpemba effect—and for the inverse Mpemba effect, in which the initially cooler system heats sooner—to emerge, the initially hotter sample must have a sufficiently larger value of excess kurtosis $a_2^0$; the larger $a_2^0$ is, the larger the cooling rate becomes. This behavior is completely analogous to that found in a granular gas of smooth hard spheres.[21]

The above analysis entails that the Mpemba effect is absent if both samples, A and B, are initially at equilibrium. In that case, $a_{2A}^0 = a_{2B}^0 = 0$, and the parameter $R^0$ defined in Eq. (4.4) diverges to infinity. For the Mpemba effect to emerge, we need to prepare the samples in nonequilibrium states before coupling them to the common reservoir at temperature $T_s$. This can be achieved, for instance, by temporarily coupling the samples to their respective reservoirs at temperatures different from $T_s$.

Analytical predictions have been obtained, in a wide range of values of the system parameters, within a linearized model. The linearization is carried around a reference temperature—specifically the initial temperature of the sample that is closer to the equilibrium value, not around the steady temperature. Therefore, our analytical framework is not limited to near-equilibrium situations. Within this scheme, we have found semi-quantitatively accurate expressions for (i) the crossover time, (ii) the maximum value of the initial temperature difference, and (iii) the magnitude of the Mpemba effect. In addition, we have looked into the limitations of the linearized model, especially for small values of the parameter $\gamma$ characterizing the nonlinearity.

This work also opens avenues for further research. It is interesting to consider in more detail some specific limits of the present model, which are physically relevant: (i) small nonlinearity $\gamma \ll 1$, which appears naturally as the first correction to the usual linear drag and (ii) time scale separation between viscous drag and collisions, i.e., either $\zeta_0^* \ll 1$ or $\zeta_0^* \gg 1$. In both cases, a systematic—mainly perturbative—analytical approach seems to be feasible. In addition, it is important to deepen our understanding of the aging phenomena in this molecular gas. Specifically, looking into the Kovacs effect,[51,52] which has attracted a lot of attention lately,[17,18,30,53–63] is compelling.

Finally, we plan to check the theoretical predictions of this work against computer simulations obtained from the Langevin equation with an interpretation of the multiplicative noise[33,64–66] consistent with the Enskog–Fokker–Planck equation (2.6).

## ACKNOWLEDGMENTS

Professor Jason Reese was a brilliant scientist in the field of kinetic theory, with very important contributions at both the theoretical and the computational level. With this paper, we respectfully pay tribute to his memory. A.S. and A.P. acknowledge financial support from the Spanish Agencia Estatal de Investigación through Grant Nos. FIS2016-76359-P and PGC2018-093998-B-I00, respectively. A.S. is also grateful to the Junta de Extremadura (Spain) for Grant No. GR18079. All the grants are partially financed by the European Regional Development Fund.

## APPENDIX A: HARD INTERACTION BETWEEN BROWNIAN PARTICLES AND BACKGROUND FLUID

In Refs. 34–36, the authors consider the emergence of nonlinear Brownian motion when an ensemble of "heavy" Brownian particles (mass $m$ and number density $n$) moves in a bath modeled as a dilute gas of "light" particles (mass $m_{\text{bf}}$ and number density $n_{\text{bf}}$), which is at equilibrium at temperature $T_s$. A velocity-dependent drag coefficient $\zeta(v)$ is obtained as an expansion in powers of the mass ratio $m_{\text{bf}}/m$, which is formally assumed to be small.

The coefficients of the expansion of $\zeta(v)$ are given in terms of integrals that involve the differential cross section for the interaction between the Brownian particles and the bath particles. Explicit expressions for $\zeta(v)$ can be derived when simple potentials are employed for this interaction. For example, all particles are considered to be three-dimensional hard spheres in Ref. 36, both the

Brownian particles and the particles in the background dilute gas. With this assumption, it is found that

$$\zeta(v) = \frac{8}{15} n_{\rm bf} S \sqrt{\frac{2m_{\rm bf}}{\pi k_B T_{\rm s}}} \frac{m_{\rm bf} v^2/2 + 5k_B T_{\rm s}}{m + m_{\rm bf}}. \tag{A1}$$

Here, $S$ is the total cross section, i.e.,

$$S = \frac{\pi(\sigma + \sigma_{\rm bf})^2}{4}, \tag{A2}$$

where $\sigma$ and $\sigma_{\rm bf}$ are the diameters of the Brownian particles and the background fluid particles, respectively. Equation (A1) is valid up to order $(m_{\rm bf}/m)^{3/2}$ and for not too large velocities, i.e., velocities that lie in the thermal range $mv^2/2k_B T_{\rm s} = O(1)$.

By comparing Eq. (A2) with Eq. (2.7), we have

$$\zeta_0 = \frac{2}{3} n_{\rm bf} (\sigma + \sigma_{\rm bf})^2 \sqrt{\frac{\pi k_B T_{\rm s}}{m}} \frac{\sqrt{2m m_{\rm bf}}}{m + m_{\rm bf}}, \tag{A3}$$

which is proportional to $\sqrt{T_{\rm s}}$, and

$$\gamma = \frac{m_{\rm bf}}{10m}, \tag{A4}$$

which is expected to be small.

In the framework developed in this paper, we measure time in terms of the number of collisions of Brownian particles among themselves. Therefore, our evolution equations involve the dimensionless low-velocity drag coefficient $\zeta_0^* = \zeta_0 \tau_{\rm s}$, introduced in Eq. (3.7). For hard spheres ($d = 3$) in the Boltzmann limit [$g(\sigma) = 1$], the characteristic time $\tau_{\rm s}$ for Brownian–Brownian collisions is

$$\tau_{\rm s}^{-1} = 2n\sigma^2 \sqrt{\frac{\pi k_B T_{\rm s}}{m}}. \tag{A5}$$

Straightforward algebraic manipulation leads to

$$\zeta_0^* = \frac{2n_{\rm bf}}{3n} \left(1 + \frac{\sigma_{\rm bf}}{\sigma}\right)^2 \frac{\sqrt{5\gamma}}{1 + 10\gamma}. \tag{A6}$$

Therefore, we have that $\zeta_0^*$ depends on three dimensionless quantities—the density ratio $n_{\rm bf}/n$, the diameter ratio $\sigma_{\rm bf}/\sigma$, and the mass ratio $m_{\rm bf}/m$, as measured by $\gamma$. This means that, even in the "natural" heavy Brownian limit $m_{\rm bf}/m \ll 1$ or $\gamma \ll 1$, $\zeta_0^*$ varies across a large range of values. For a given problem, its specific value depends on $n_{\rm bf}/n$ and $\sigma_{\rm bf}/\sigma$, but not on the steady temperature. The ratio of time scales associated with the viscous drag and Brownian–Brownian collisions is thus independent of the temperature of the bath.

The simple expressions for $\gamma$ and $\zeta_0^*$, Eqs. (A4) and (A6), hold for hard-sphere interaction in the Boltzmann limit. More complicated behaviors may be found in other situations, but we expect the qualitative picture derived here to be still valid. As a consequence while the range of $\gamma$ is somehow limited, that of $\zeta_0^*$ is not necessarily so. This explains why we have restricted ourselves to $\gamma \leq 0.2$ throughout the paper but treated $\zeta_0^*$ as an independent parameter, which may attain both small and large values.

## APPENDIX B: SOLUTION OF THE LINEARIZED SYSTEM

Our starting point is the nonlinear system (3.6), written in the Sonine approximation. First, we introduce the deviation of temperature from a certain reference temperature $\theta_r$ by

$$\Psi(t^*) = \theta(t^*) - \theta_r. \tag{B1}$$

Second, we linearize Eq. (3.6) with respect to $\Psi(t^*)$ and $a_2(t^*)$. Note that Eq. (3.6) is linear in $a_2$ but nonlinear in $\theta$ and, in addition, the "coefficients" of $a_2$ are functions of $\theta$. The result is

$$\begin{pmatrix} \dot{\Psi} \\ \dot{a}_2 \end{pmatrix} = -\begin{pmatrix} \Lambda_{11} & \Lambda_{12} \\ \Lambda_{21} & \Lambda_{22} \end{pmatrix} \cdot \begin{pmatrix} \Psi \\ a_2 \end{pmatrix} + \begin{pmatrix} C_1 \\ C_2 \end{pmatrix}, \tag{B2}$$

where

$$C_1 = 2\zeta_0^* (1 - \theta_r)[1 + \gamma(d+2)\theta_r], \tag{B3a}$$

$$C_2 = 8\zeta_0^* \gamma (1 - \theta_r), \tag{B3b}$$

and $\Lambda_{ij}$ has been defined in Eq. (4.1). The solution of the simplified linear model (B2) yields

$$\Psi(t^*) = D_1 + \frac{(\lambda_+ - \Lambda_{11})(\Psi^0 - D_1) - \Lambda_{12}(a_2^0 - D_2)}{\delta_\lambda e^{\lambda_- t^*}} - \frac{(\lambda_- - \Lambda_{11})(\Psi^0 - D_1) - \Lambda_{12}(a_2^0 - D_2)}{\delta_\lambda e^{\lambda_+ t^*}}, \tag{B4a}$$

$$a_2(t^*) = D_2 + \frac{(\lambda_+ - \Lambda_{22})(a_2^0 - D_2) - \Lambda_{21}(\theta^0 - D_1)}{\delta_\lambda e^{\lambda_- t^*}} - \frac{(\lambda_- - \Lambda_{22})(a_2^0 - D_2) - \Lambda_{21}(\theta^0 - D_1)}{\delta_\lambda e^{\lambda_+ t^*}}, \tag{B4b}$$

where $\lambda_\pm$ are the eigenvalues of the matrix $\Lambda$ defined in Eq. (4.2), and we have defined the parameters

$$D_1 = \frac{\Lambda_{22} C_1 - \Lambda_{12} C_2}{\Lambda_{11}\Lambda_{22} - \Lambda_{12}\Lambda_{21}}, \quad D_2 = \frac{\Lambda_{11} C_2 - \Lambda_{21} C_1}{\Lambda_{11}\Lambda_{22} - \Lambda_{12}\Lambda_{21}}. \tag{B5}$$

Neither $\Psi$ nor $a_2$ reaches its actual equilibrium value in the long-time limit, unless $\theta_r = 1$. This is not a problem for the analysis carried out in the main text because this linear theory is only used for the early stage of the time evolution, in which the Mpemba effect may emerge.

Now, let us consider two different initial states: A, with initial values of the temperature and the excess kurtosis $\{\theta_A^0, a_{2A}^0\}$, and B, with initial values $\{\theta_B^0, a_{2B}^0\}$. The linear theory makes it possible to write analytical predictions for the differences between their respective time evolutions, i.e., $\Delta\theta(t^*) = \theta_A(t^*) - \theta_B(t^*) = \Psi_A(t^*) - \Psi_B(t^*)$ and $\Delta a_2(t^*) = a_{2A}(t^*) - a_{2B}(t^*)$. Making use of Eq. (B4), we arrive precisely at Eq. (4.3) in the main text.

## DATA AVAILABILITY

The data that support the findings of this study are available from the corresponding author upon reasonable request.

## REFERENCES


[1]N. C. Keim, J. D. Paulsen, Z. Zeravcic, S. Sastry, and S. R. Nagel, "Memory formation in matter," Rev. Mod. Phys. **91**, 035002 (2019).
[2]J. P. Bouchaud, "Weak ergodicity breaking and aging in disordered systems," J. Phys. I **2**, 1705–1713 (1992).
[3]J. J. Brey and A. Prados, "Stretched exponential decay at intermediate times in the one-dimentional Ising model at low temperatures," Physica A **197**, 569–582 (1993).
[4]J. J. Brey and A. Prados, "Dynamical behavior of a one-dimensional Ising model submitted to continuous heating and cooling processes," Phys. Rev. B **49**, 984–997 (1994).
[5]C. A. Angell, K. L. Ngai, G. B. McKenna, P. F. McMillan, and S. W. Martin, "Relaxation in glassforming liquids and amorphous solids," J. Appl. Phys. **88**, 3113–3157 (2000).
[6]F. Ritort and P. Sollich, "Glassy dynamics of kinetically constrained models," Adv. Phys. **52**, 219–342 (2003).
[7]A. R. Jacob, E. Moghimi, and G. Petekidis, "Rheological signatures of aging in hard sphere colloidal glasses," Phys. Fluids **31**, 087103 (2019).
[8]G. J. M. Koper and H. J. Hilhorst, "Nonequilibrium dynamics and aging in a one-dimensional Ising spin glass," Physica A **155**, 431–459 (1989).
[9]L. F. Cugliandolo, J. Kurchan, and F. Ritort, "Evidence of aging in spin-glass mean-field models," Phys. Rev. B **49**, 6331–6334 (1994).
[10]A. Prados, J. J. Brey, and B. Sánchez-Rey, "Aging in the one-dimensional Ising model with Glauber dynamics," Europhys. Lett. **40**, 13–18 (1997).
[11]L. Berthier and J.-P. Bouchaud, "Geometrical aspects of aging and rejuvenation in the Ising spin glass: A numerical study," Phys. Rev. B **66**, 054404 (2002).
[12]J. J. Brey, A. Prados, M. I. García de Soria, and P. Maynar, "Scaling and aging in the homogeneous cooling state of a granular fluid of hard particles," J. Phys. A: Math. Theor. **40**, 14331–14342 (2007).
[13]S. R. Ahmad and S. Puri, "Velocity distributions and aging in a cooling granular gas," Phys. Rev. E **75**, 031302 (2007).
[14]C. Josserand, A. V. Tkachenko, D. M. Mueth, and H. M. Jaeger, "Memory effects in granular materials," Phys. Rev. Lett. **85**, 3632–3635 (2000).
[15]J. J. Brey and A. Prados, "Linear response of vibrated granular systems to sudden changes in the vibration intensity," Phys. Rev. E **63**, 061301 (2001).
[16]R. Hecht, S. F. Cieszymski, E. V. Colla, and M. B. Weissman, "Aging dynamics in ferroelectric deuterated potassium dihydrogen phosphate," Phys. Rev. Mater. **1**, 044403 (2017).
[17]Y. Lahini, O. Gottesman, A. Amir, and S. M. Rubinstein, "Nonmonotonic aging and memory retention in disordered mechanical systems," Phys. Rev. Lett. **118**, 085501 (2017).
[18]S. Dillavou and S. M. Rubinstein, "Nonmonotonic aging and memory in a frictional interface," Phys. Rev. Lett. **120**, 224101 (2018).
[19]E. B. Mpemba and D. G. Osborne, "Cool?," Phys. Educ. **4**, 172–175 (1969).
[20]Z. Lu and O. Raz, "Nonequilibrium thermodynamics of the Markovian Mpemba effect and its inverse," Proc. Natl. Acad. Sci. U. S. A. **114**, 5083–5088 (2017).
[21]A. Lasanta, F. Vega Reyes, A. Prados, and A. Santos, "When the hotter cools more quickly: Mpemba effect in granular fluids," Phys. Rev. Lett. **119**, 148001 (2017).
[22]I. Klich, O. Raz, O. Hirschberg, and M. Vucelja, "Mpemba index and anomalous relaxation," Phys. Rev. X **9**, 021060 (2019).
[23]M. Baity-Jesi, E. Calore, A. Cruz, L. A. Fernandez, J. M. Gil-Narvión, A. Gordillo-Guerrero, D. Iñiguez, A. Lasanta, A. Maiorano, E. Marinari, V. Martin-Mayor, J. Moreno-Gordo, A. Muñoz Sudupe, D. Navarro, G. Parisi, S. Perez-Gaviro, F. Ricci-Tersenghi, J. J. Ruiz-Lorenzo, S. F. Schifano, B. Seoane, A. Tarancón, R. Tripiccione, and D. Yllanes, "The Mpemba effect in spin glasses is a persistent memory effect," Proc. Natl. Acad. Sci. U. S. A. **116**, 15350–15355 (2019).
[24]Z.-Y. Yang and J.-X. Hou, "Non-Markovian Mpemba effect in mean-field systems," Phys. Rev. E **101**, 052106 (2020).
[25]*The Works of Aristotle (Translated into English Under the Editorship of W. D. Ross)*, edited by W. D. Ross (Oxford Clarendon Press, 1931), Vol. III.
[26]H. C. Burridge and P. F. Linden, "Questioning the Mpemba effect: Hot water does not cool more quickly than cold," Sci. Rep. **6**, 37665 (2016).
[27]A. Gijón, A. Lasanta, and E. R. Hernández, "Paths towards equilibrium in molecular systems: The case of water," Phys. Rev. E **100**, 032103 (2019).
[28]A. Torrente, M. A. López-Castaño, A. Lasanta, F. Vega Reyes, A. Prados, and A. Santos, "Large Mpemba-like effect in a gas of inelastic rough hard spheres," Phys. Rev. E **99**, 060901(R) (2019).
[29]A. Biswas, V. V. Prasad, O. Raz, and R. Rajesh, "Mpemba effect in driven granular Maxwell gas," arXiv:2004.11559 (2020).
[30]E. Mompó, M. A. López Castaño, A. Torrente, F. Vega Reyes, and A. Lasanta, "Memory effects in a gas of viscoelastic particles," arXiv:2006.00241 (2020).
[31]F. Vega Reyes and A. Santos, "Steady state in a gas of inelastic rough spheres heated by a uniform stochastic force," Phys. Fluids **27**, 113301 (2015).
[32]A. Lasanta, F. Vega Reyes, V. Garzó, and A. Santos, "Intruders in disguise: Mimicry effect in granular gases," Phys. Fluids **31**, 063306 (2019).
[33]Y. L. Klimontovich, "Nonlinear Brownian motion," Phys.-Usp. **37**, 737–767 (1994).
[34]L. Ferrari, "Particles dispersed in a dilute gas: Limits of validity of the Langevin equation," Chem. Phys. **336**, 27–35 (2007).
[35]L. Ferrari, "Particles dispersed in a dilute gas. II. From the Langevin equation to a more general kinetic approach," Chem. Phys. **428**, 144–155 (2014).
[36]M. Hohmann, F. Kindermann, T. Lausch, D. Mayer, F. Schmidt, E. Lutz, and A. Widera, "Individual tracer atoms in an ultracold dilute gas," Phys. Rev. Lett. **118**, 263401 (2017).
[37]J. E. Stout, S. P. Arya, and E. L. Genikhovich, "The effect of nonlinear drag on the motion and settling velocity of heavy particles," J. Atmos. Sci. **52**, 3836–3848 (1995).
[38]J. C. H. Fung, "Effect of nonlinear drag on the settling velocity of particles in homogeneous isotropic turbulence," J. Geophys. Res. **103**, 27905–27917, https://doi.org/10.1029/98jc02822 (1998).
[39]F. Maggi, "The settling velocity of mineral, biomineral, and biological particles and aggregates in water," J. Geophys. Res. Oceans **118**, 2118–2132, https://doi.org/10.1002/jgrc.20086 (2013).
[40]A. R. Plastino, R. S. Wedemann, E. M. F. Curado, F. D. Nobre, and C. Tsallis, "Nonlinear drag forces and the thermostatistics of overdamped motion," Phys. Rev. E **98**, 012129 (2018).
[41]S. Chapman and T. G. Cowling, *The Mathematical Theory of Non-Uniform Gases*, 3rd ed. (Cambridge University Press, Cambridge, UK, 1970).
[42]C. Cercignani, *The Boltzmann Equation and Its Applications* (Springer-Verlag, New York, 1988).
[43]*Handbook of Mathematical Functions*, edited by M. Abramowitz and I. A. Stegun (Dover, New York, 1972).
[44]T. P. C. van Noije and M. H. Ernst, "Velocity distributions in homogeneous granular fluids: The free and the heated case," Granular Matter **1**, 57–64 (1998).
[45]J. M. Montanero and A. Santos, "Computer simulation of uniformly heated granular fluids," Granular Matter **2**, 53–64 (2000).
[46]A. Santos and J. M. Montanero, "The second and third Sonine coefficients of a freely cooling granular gas revisited," Granular Matter **11**, 157–168 (2009).
[47]P. Résibois and M. de Leener, *Classical Kinetic Theory of Fluids* (John Wiley & Sons, New York, 1977).
[48]*Granular Gases*, Lecture Notes in Physics Vol. 564, edited by T. Pöschel and S. Luding (Springer, Berlin, 2001).
[49]Throughout, the superscript 0 denotes initial value for all the variables.
[50]A similar observation was found in Ref. 21 for a granular fluid of smooth hard particles.
[51]A. J. Kovacs, "Transition vitreuse dans les polymères amorphes. Etude phénoménologique," Fortschr. Hochpolym.-Forsch. **3**, 394–507 (1963).
[52]A. J. Kovacs, J. J. Aklonis, J. M. Hutchinson, and A. R. Ramos, "Isobaric volume and enthalpy recovery of glasses. II. A transparent multiparameter theory," J. Polym. Sci., Polym. Phys. Ed. **17**, 1097–1162 (1979).
[53]A. Prados and J. J. Brey, "The Kovacs effect: A master equation analysis," J. Stat. Mech.: Theory Exp. **2010**, P02009.
[54]E. Bouchbinder and J. S. Langer, "Nonequilibrium thermodynamics of the Kovacs effect," Soft Matter **6**, 3065–3073 (2010).

[55]G. Diezemann and A. Heuer, "Memory effects in the relaxation of the Gaussian trap model," Phys. Rev. E **83**, 031505 (2011).
[56]Y.-C. Chang, C. Wang, S. Yin, R. C. Hoffman, and A. G. Mott, "Kovacs effect enhanced broadband large field of view electro-optic modulators in nanodisordered KTN crystals," Opt. Express **21**, 17760–17768 (2013).
[57]A. Prados and E. Trizac, "Kovacs-like memory effect in driven granular gases," Phys. Rev. Lett. **112**, 198001 (2014).
[58]E. Trizac and A. Prados, "Memory effect in uniformly heated granular gases," Phys. Rev. E **90**, 012204 (2014).
[59]M. Ruiz-García and A. Prados, "Kovacs effect in the one-dimensional Ising model: A linear response analysis," Phys. Rev. E **89**, 012140 (2014).
[60]L. Berthier, D. Coslovich, A. Ninarello, and M. Ozawa, "Equilibrium sampling of hard spheres up to the jamming density and beyond," Phys. Rev. Lett. **116**, 238002 (2016).
[61]R. Kürsten, V. Sushkov, and T. Ihle, "Giant Kovacs-like memory effect for active particles," Phys. Rev. Lett. **119**, 188001 (2017).
[62]A. Lasanta, F. Vega Reyes, A. Prados, and A. Santos, "On the emergence of large and complex memory effects in nonequilibrium fluids," New J. Phys. **21**, 033042 (2019).
[63]M. Lulli, L.-H. Zhang, C.-S. Lee, H.-Y. Deng, and C.-H. Lam, "Kovacs effect studied using the distinguishable particles lattice model of glass," arXiv:1910.10374 (2019).
[64]J. M. Sancho, M. San Miguel, S. L. Katz, and J. D. Gunton, "Analytical and numerical studies of multiplicative noise," Phys. Rev. A **26**, 1589–1609 (1982).
[65]N. G. V. Kampen, *Stochastic Processes in Physics and Chemistry* (North-Holland, Amsterdam, 2007).
[66]R. Mannella and P. V. E. McClintock, "Itô versus Stratonovich: 30 years later," Fluctuation Noise Lett. **11**, 1240010 (2012).